Iranian Polymer Journal (2024) 33:1031–1046
https://doi.org/10.1007/s13726-024-01304-x

ORIGINAL RESEARCH

Reactive extrusion foaming of poly(lactic acid): tailoring foam properties through controlling in-process chemical reactions

Maryam Valipour[1] · Mahdi Rahmanifard[2] · Navid Jaberi[3] · Alireza Shadman[4] · Mehdi Hatami[1] · Hossein Ali Khonakdar[3] · Farkhondeh Hemmati[2]

Received: 24 October 2023 / Accepted: 15 January 2024 / Published online: 1 April 2024

Abstract

A continuous extrusion foaming process was performed on poly(lactic acid) (PLA) in the presence of different chemical foaming agents (CFAs) and a chain extender additive using different extruder barrel and die temperature profiles. Chemical reactions, which are involved in the extrusion foaming process of PLA, are intensely investigated to control the reactive extrusion process and tailor the foam final properties. A set of experiments was designed using the response surface methodology to evaluate the effects of material and processing parameters and optimize the PLA foam property. The results showed that the maximum void fraction, i.e. 0.55, was obtained by exothermic CFA at higher extruder temperatures. In contrast to the exothermic CFA, the addition of endothermic CFAs did not result in lightweight biodegradable foams. The void fractions of these extruded foams were less than 0.05. The presence of water molecules as a by-product of the decomposition reaction and also relatively lower decomposition temperatures of the endothermic CFAs have been considered as the main reasons. Among the variables studied, the CFA type had the strongest impact on the foam properties. In the second step, the barrel and die temperatures were adjusted accordingly.

Graphical abstract

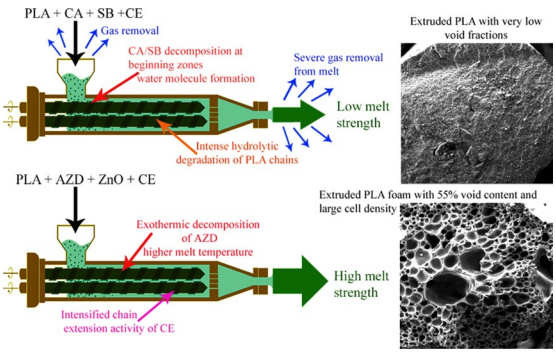

Keywords Foam · Poly(lactic acid) · Chemical foaming agent · Extrusion · Response surface method

Introduction

Due to serious environmental problems accompanied by plastic waste, researchers around the world have sought to produce biodegradable plastics [1–3]. Among biopolymers, poly(lactic acid) (PLA) is a renewable biopolymer that is produced from corn, rice, wheat, potato, sugarcane and bagasse [4, 5]. PLA has excellent Young's modulus, high strength, and good processability compared to other biopolymers [1], and its products can be obtained through common plastic processing techniques such as injection molding and extrusion [4, 6]. The production of PLA reached 293,000 tons in 2019 and its consumption market has an increasing trend [7]. Nonetheless, PLA has disadvantages such as brittleness, low toughness, slow crystallization kinetics, and

Extended author information available on the last page of the article

low melt strength [8, 9]. Therefore, improving various properties including rheological and viscoelastic properties of PLA melt in various applications including foams is very important [10]. Thereby, the PLA foams can be considered as the most promising replacement for the synthetic plastic foams like polystyrene. The PLA foams are also biodegradable, though their biodegradation rate is found to be lower than that of unfoamed PLA products, owing to the necessity of the hydration of the expandable microsphere and polymer matrix interface [11]

The underlying mechanism governing the low melt strength of PLA in different foaming processes is the low thermal stability of bioplastic PLA. This thermoplastic undergoes thermal degradation and dominant chain scission under stress-induced flow fields in the molten state. As a direct result of the chain scission mechanism, the average molecular weight of PLA chains, melt viscosity and melt strength of PLA diminish. With low viscoelastic properties, PLA melt cannot resist the extensional stresses during the bubble growth stage of the foaming process. Therefore, severe structure collapse and gas escape occur [12].

During the last two decades, the effects of epoxy-based chain extenders, various nanoparticles, and different physical and chemical foaming agents on the processability and properties of the PLA foams have been investigated by various researchers [13, 14]. The low melt strength of PLA has an adverse effect on the growth of foam cells and often results in the intense structural collapse and gas removal from the melt. One of the commonly used solutions to solve the problem of low melt strength is to add a chain extender (CE) to PLA [6]. It has been reported that the foamability of PLA in the solvent-free reactive extrusion foaming process can be improved by adding peroxide initiators and tri-functional crosslinking and chain extender additives [15]. The improvements in the foamability may result from long-branching reaction, higher crystallinity degree, faster crystallization process and larger melt strength [15]. In the molten state, the chain extender reacts with the hydroxyl or carboxyl end groups of PLA chains and the linear PLA chains change into long-branched macromolecules with larger molecular weight and higher melt strength [16]. The effects of adding an epoxy-based CE on the processability and properties of PLA foams were investigated by Kozlowski and Ludwiczak in 2015 [17]. The findings of this study showed that the melt viscosity and cold crystallization temperature of PLA are enhanced by adding the CE additive [17]. Julien et al. [18] in 2015 also prepared PLA/chain extender foams at different concentrations of CE using a single-screw extruder. Their results showed that the addition of CE increases the average molecular weight, melt viscosity and viscoelastic properties. Blending CE with PLA also resulted in a decrease in void fraction and average cell size and an increase in cell density [18]. Recently, the bead foams of modified PLA with CE have been prepared by one-step anhydrous supercritical carbon dioxide extrusion process [19]. The applied process has shortened the production time and prevented the PLA hydrolysis and wastewater generation. The chain extension activity of CE increased the PLA's melt strength from 0.8 to 16.7 cN, leading to a PLA bead foam with larger expansion ratio [19].

Besides the given additive, the type of chemical foaming agent (CFA) has also a profound impact on the foamability of PLA melt. The effects of adding an endothermic chemical foaming agent on the structural properties of PLA extrusion foams were investigated by Julien et al. [18]. In this research, PLA master batch containing sodium bicarbonate and citric acid was used for PLA foaming in the form of films. By increasing the content of endothermic foaming agent, cell density and bubble size in the PLA matrix decreased [18]. In a similar study, Kmetty et al. in 2018 investigated the effects of endothermic chemical foaming agents (mixture of sodium bicarbonate and citric acid) and an exothermic chemical foaming agent (azodicarbonamide) (AZD) on the foaming behaviour of PLA melt through the extrusion process [22]. Based on the morphological results, the lowest foam density and the highest cell density were obtained in the foams containing the exothermic foaming agent [22].

Along with different additives that can positively alter the foamability of PLA melt, the deep influence of melt temperature and set processing temperature on PLA foam properties has been reported [20]. The effects of processing temperature and foaming agent content on the physical and mechanical properties of PLA/kenaf fiber (KF) composites prepared through the extrusion process were investigated in a research by Nur Adilah et al. [13] in 2018. The morphological observations showed that the cell size of foamed PLA/KF composites became larger when the extruder temperature profile increased [13]. In a similar study, Litauszki et al. [14], in 2020, investigated the effects of different chemical foaming agents and extruder temperature profiles on the microstructure of PLA-based foams obtained from the extrusion foaming process. According to the test results, low-weight PLA foam was achieved at a process temperature of 190 °C. In this work, at high contents of foaming agent (4% and 8% by weights) and high process temperatures (210 and 230 °C), the cell wall rupture occurred, which led to the formation of larger cells [14]. In a recently published work, the effects of the extrusion temperature and material feed rate on the foamability of PLA were studied during 3D printing process [21]. Their findings confirmed that at higher processing temperatures, the number of bubble nucleation sites caused by the foaming agent and the cells growth rate increased [21].

The continuous extrusion foaming process of PLA has been studied by several groups, owing to the process relevance for scaling up to an industrial scale [18, 22]. In the

continuous extrusion foaming process of PLA melt in the presence of chemical foaming agent and CE additives, a series of chemical reactions occur simultaneously, including chain scission of PLA chains, chain extension reaction of CE with PLA chains and decomposition of CFA. These reactions make the control of the extrusion foaming process challenging and complex. Each of these chemical reactions can influence the intensity of other reactions. Therefore, the main objective of the current work is the study of these concurrent reactions and their interactions in the extrusion foaming of PLA. To acquire an insight into the details of PLA chemical extrusion foaming process, simultaneous effects of different exothermic and endothermic chemical foaming agents, chain extender level and extruder temperature profile and their interactions on the physical and structural properties of PLA foams have been quantitatively studied using a suitable experimental design. Although the effects of CFA type, the content of common CEs in the polyester extrusion processes, and melt temperature on the PLA foamability have been investigated individually in previous published works, the simultaneous influence of these variables on the chemical foaming of the PLA melt through a one-step melt extrusion process and mathematical modelling of the extruded foam properties, to the best of our knowledge, have not been yet studied.

Experimental

Materials

A poly(lactic acid) (PLA), Ö5 BIOKAS grade, with a glass transition temperature (T_g) of 60.4 °C, melting point (T_m) of 146.8 °C and melt flow index of 7 g/10 min (210 °C, 2.16 kg) was obtained from Chemikas Co. (Austria). The exothermic CFA used in this study was azodicarbonamide (7000 dB, 97% pure), supplied by Kum Yang Co. (South Korea). Zinc oxide (ZnO, above 98% pure) produced by Merck (Germany), was used to activate the exothermic foaming agent and decompose it at lower temperatures. The content of zinc oxide at 0.25 phr was constant in all samples. Sodium bicarbonate (SB, 106,329 grade, $NaHCO_3$, more than 99% pure) and citric acid (CA, 100,247 grade, $C_6H_8O_7$, more than 99% pure) were used as endothermic chemical foaming agents produced by Merck (Germany). A multipurpose acrylic styrenic chain extender, Joncryl ADR 4400 grade from BASF (Germany), with a molecular weight of 8400–5800 g/mol was used to improve the foamability of the PLA melt. Tetrahydrofuran (THF, above 99.8% pure) solvent produced by Merck (Germany) was also used for measuring the gel content of the foams.

Sample preparation

In this work, the D-optimal design from response surface methodology was applied as an efficient experimental design with three different variables including the content of chain extender, the type of foaming agent and extruder temperature profile. The studied variables along with the levels are given in Table 1. Three amounts of chain extender, three different extruder temperatures and three different combinations of foaming agents were considered. The content of foaming agents in all the prepared samples was 4 phr. In the samples in which two exothermic and endothermic foaming agents were used together, the amount of these foaming agents was equal (2 phr + 2 phr). Based on D-optimal design, a set of 20-trial design was employed. The design is shown in Table 2. Based on the literature, the mentioned design variables are among the most important factors affecting the processability of PLA foams in a one-step continuous extrusion process.

For PLA foaming, the foam samples were prepared according to the predetermined experimental design given in Table 2. The codes of the prepared foam samples are defined in this table. The foam sample codes start with F letter. Twenty samples with different concentrations of CE, different types of CFA at three different extruder temperature profiles were extruded. The chemical foaming agent included azodicarbonamide (AZD) as an exothermic foaming agent, citric acid (CA) with sodium bicarbonate (SB) as endothermic foaming agents and a combination of these exothermic and endothermic foaming agents in equal amounts. Three different extruder temperature profiles of 140–145–160–160–160 °C (named as 160), 140–145–160–175–175 °C (named as 175), and 140–145–160–190–190 °C (named as 190) (from hopper to die) were applied. The PLA foams were extruded using a twin-screw co-rotating extruder (Rondolmicro compounder, UK) with a screw speed of 150 rpm equipped with a rod-shaped die.

In addition to the prepared foams, unfoamed samples, with similar formulations and without the use of chemical foaming agents, were prepared as control samples under the same processing conditions. The formulations of these control samples are also given in Table 2. In Table 2, the UF letters at the beginning of sample codes are related to

Table 1 Experimental design variables and the variable levels

Variable	Factor	Level		
		1	2	3
CE content (phr)	A	0.5	1	2
Temperature profile (°C)	B	160	175	190
CFA type	C	AZD	AZD + CA/SB	CA/SB

Table 2 Formulations and process temperature of foamed and unfoamed PLA samples

No	Sample code	CE content (phr)	CFA type (CFA content(phr))	ZnO content(phr)	Temperature profile (°C)
1	F-CE0.5/CASB/175	0.5	CA (2) + SB (2)	–	175
2	UF-CE0.5/175	0.5	–	–	175
3	F-CE0.5/CASB/175	0.5	CA (2) + SB (2)	–	175
4	UF-CE0.5/175	0.5	–	–	175
5	F-CE0.5/AZD/175	0.5	AZD (4)	0.25	175
6	UF-CE0.5/175	0.5	–	–	175
7	F-CE2/CASB/175	2	CA (2) + SB (2)	–	175
8	UF-CE2/175	2	–	–	175
9	F-CE0.5/AZD/160	0.5	AZD (4)	0.25	160
10	UF-CE0.5/160	0.5	–	–	160
11	F-CE2/AZDCASB/190	2	AZD (2) + CA (1) + SB (1)	0.25	190
12	UF-CE2/190	2	–	–	190
13	F-CE2/AZD/190	2	AZD (4)	0.25	190
14	UF-CE2/190	2	–	–	190
15	F-CE1/CASB/190	1	CA (2) + SB (2)	–	190
16	UF-CE1/190	1	–	–	190
17	F-CE1/CASB/190	1	CA (2) + SB (2)	–	190
18	UF-CE1/190	1	–	–	190
19	F-CE0.5/AZD/190	0.5	AZD (4)	0.25	190
20	UF-CE0.5/190	0.5	–	–	190
21	F-CE2/AZD/175	2	AZD (4)	0.25	175
22	UF-CE2/175	2	–	–	175
23	F-CE1/AZD/175	1	AZD (4)	0.25	175
24	UF-CE1/175	1	–	–	175
25	F-CE2/AZDCASB/160	2	AZD (2) + CA (1) + SB (1)	0.25	160
26	UF-CE2/160	2	–	–	160
27	F-CE0.5/AZDCASB/160	0.5	AZD (2) + CA (1) + SB (1)	0.25	160
28	UF-CE0.5/160	0.5	–	–	160
29	F-CE2/CASB/175	2	CA (2) + SB (2)	–	175
30	UF-CE2/175	2	–	–	175
31	F-CE1/CASB/160	1	CA (2) + SB (2)	–	160
32	UF-CE1/160	1	–	–	160
33	F-CE1/AZD/190	1	AZD (4)	0.25	190
34	UF-CE1/190	1	–	–	190
35	F-CE0.5/AZDCASB/190	0.5	AZD (2) + CA (1) + SB (1)	0.25	190
36	UF-CE0.5/190	0.5	–	–	190
37	F-CE2/AZD/160	2	AZD (4)	0.25	160
38	UF-CE2/160	2	–	–	160
39	F-CE1/CASB/160	1	CA (2) + SB (2)	–	160
40	UF-CE1/160	1	–	–	160

the unfoamed control samples. For instance, in F-CEα/βγδ/θ or UF-CEα/θ sample code, α shows the chain extender content, βγδ stand for the name/names of the chemical foaming agent/agents in the foam samples and θ defines the extruder temperature profile. Before the extrusion process, the raw materials of foams and unfoamed samples were dried in a vacuum oven at a temperature of 60 °C for 12 h.

Characterization

The densities of foamed and unfoamed samples were measured following the ASTM D3575 and ASTM D792 standards, respectively. The densities were calculated according to Eqs. (1)and (2). The density of foam samples was determined by measuring the weight and volume of the rod-shaped specimens. For unfoamed samples, the

measurement was based on the solvent displacement method and methanol was used as the medium. The void fraction of foams was calculated according to ASTM D2734 standard (Eq. 3):

$$\text{Density of foam} = \frac{m}{v} \tag{1}$$

$$\text{Density of unfoamed sample} = \frac{m_{\text{air}}}{m_{\text{air}} - m_{\text{solvent}}} \times \rho_{\text{methanol}} \tag{2}$$

$$\text{Void fraction} = \frac{\rho_{\text{unfoam}} - \rho_{\text{foam}}}{\rho_{\text{unfoam}}} \tag{3}$$

where ρ_{unfoam} and ρ_{foam} are the densities of unfoamed and foamed samples at the same CE content and temperature profile, respectively. Additionally, m is the mass of foamed sample and v is the volume of the foamed specimen, m_{air} is the mass of the sample in air,m_{solvent} is the mass of the sample in methanol, ρ_{methanol} is the density of methanol at temperature of the experiment. The data are reported as the average of at least three replicates.

A scanning electron microscope (SEM), XL 30 model Philips (Netherlands), was used to study the foam morphology on the cryo-fractured surfaces of rod-shaped specimens. For sample preparation, the foam samples were fractured in liquid nitrogen, after being kept for at least 15 min in a liquid nitrogen bath. Afterward, the cryo-fractured surfaces were subjected to gold-sputtering before the examination. Structural characteristics of foams were determined using Digimizer software and SEM images. The mentioned characteristics include the number average diameter (D_n), volume average diameter (D_v) of bubbles as well as cell density (N_c), which are calculated using Eqs. (4)–(6):

$$D_n = \frac{\sum(n_i d_i)}{\sum n_i} \tag{4}$$

$$D_v = \frac{\sum(v_i d_i)}{\sum v_i} \tag{5}$$

$$N_C = \left(\frac{n}{A}\right)^{3/2}\left(\frac{\rho_{\text{unfoam}}}{\rho_{\text{foam}}}\right) \tag{6}$$

where n_i and v_i are the number and volume of bubbles with diameter d_i, respectively; and n is the number of cells on the cryo-fractured surface of foam having area A.

In order to determine the effects of adding polymer chain extender and foaming agents on the number- and weight-average molecular weights as well as molecular weight distribution of PLA, a gel permeation chromatography (GPC) device made by Agilent Company (USA) was used. The samples were dissolved in THF solvent. The concentration of dissolved sample in the THF solvent was 1 g/L. The flow rate of eluent was 1 mL/min and the injected volume of sample was 20 µL. A RID-A refractive index signal detector was used in this device. Polystyrene standards with polydispersity index (PDI) less than 1.1 were used for GPC calibration. The number-average molecular weight ($\overline{M}_n$), weight-average molecular weight ($\overline{M}_w$), Z-average molecular weight ($\overline{M}_z$) and molecular weight distribution (PDI) were calculated for the samples.

In order to investigate the chemical reactions between the ingredients of foams during the foaming process, a Fourier transform infrared spectrometer (FTIR) made by the Bruker Tensor Company (Germany) was used. The sample solid powder was added to KBr and the pressed disk was examined. Each sample was scanned 64 times in the wavenumber range of 4000–400 cm^{-1}. Foam and granular samples were dissolved in chloroform and then precipitated in methanol. The precipitated solid samples were ground to obtain a fine powder.

The gel content of extruded samples was measured according to ASTM D2765 standard. In this experiment, the samples were dried in a vacuum oven at a temperature of 60 °C for a suitable long period to reach a constant weight. After measuring the constant weights of dried samples (W_i), the specimens were placed in THF solvent for 24 h. The specimens were placed inside aluminum mesh envelopes and put inside the solvent. After the dissolution of the uncrosslinked parts of samples, the remaining parts were dried in a vacuum oven until a constant weight (W_f) was obtained. The gel content percentage of the samples was calculated following.

Equation 7. The final value reported for the gel content of each sample was the average of three replicates.

$$\text{Gel content} = \frac{W_f}{W_i} \times 100 \tag{7}$$

The thermal stability of raw materials and foam samples was evaluated by a thermogravimetric analyzer (TGA) made by Perkin Elmer Company (USA). About 5–10 mg of each sample was placed in a platinum pan and heated from ambient temperature to 700 °C at a heating rate of 10 °C/min under a highly pure nitrogen atmosphere.

Results and discussion

Mathematical modeling of PLA foam property

Using the response surface method, as a useful tool for data analysis and optimization, the void fraction of the obtained extrusion foams against the studied variables was quantitatively studied. In the following subsection, it is shown that there is no evidence of bubbles inside

the foamed samples containing the endothermic foaming agents, namely, sodium bicarbonate and citric acid. Due to the absence of bubbles in these samples, it is not possible to quantitatively analyze the structural properties of foams such as the average cell size and cell density of all the prepared samples using RSM software. Therefore, modeling using the capabilities of RSM software was done only for the physical property of foams, i.e. void fraction. The density of foamed and unfoamed PLA samples along with their void fraction is presented in Table 3.

The data of analysis of variance (ANOVA) for the best fitted-model on void fraction response are collected in Table 4 to investigate the significance of the model. Among all the available regression models, the linear function provides the best fit with the experimental data. The significance of a model can be studied with the R-squared criterion and lack of fit test [23]. The significance of a model in ANOVA analysis is determined by an F-value in the range of 95% and a *P*-value less than 0.05 [23, 24]. The *F*-value is the mean square of a model divided by the error. The larger *F*-value and the lower *P*-value mean the model is more significant. As shown in Table 4, the *P*-value of the model is less than 0.0001 and the *F*-value is 115.75, which verify the adequacy of the model for fitting the experimental data. The R-squared value of the regression model also confirms the significance of the model, which was 97% for void fraction response here. The best-fitted regression functions for the void fraction response are represented in Table 5 for three types of CFA used here, i.e. AZD, CA/SB and AZD + CA/SB.

Figure 1 shows the predicted values of void fraction versus the actual values obtained by experimental measurements. The predicted values are obtained using a linear interpolating function yielded from RSM. The linear relationship between the data provided by the interpolation functions and the experimental results can also be used to investigate the significance of the fitted functions [23, 24]. As shown in Fig. 1, the response data in the presence of AZD have a minimal deviation from the linear relationship, which is adjusted according to the R-squared of 97%. The smallest deviation from the 45° line shows the significance of the prediction model [24].

Figure 2 shows the response contour plots of foam void fraction against variables, A and B, for different types of CFA. As can be seen in this figure, the maximum value of the void fraction is obtained at the highest temperature profile of the extruder and the AZD type of CFA. Another notable point of this figure is the insignificant effect of CE content on the void fraction of the extruded PLA foams. It can be found from the data in Table 3 that the CE content influences the void fraction of foams, though its impact is not comparable with the effects of other influential factors, including the extruder temperature profile and CFA type.

Table 3 Density and void fraction of foamed and unfoamed PLA samples

No	Sample code	Density (g/c m^3)	Void fraction
1	F-CE0.5/CASB/175	1.183 ± 0.002	0.0199
	UF-CE0.5/175	1.207 ± 0.002	–
2	F-CE0.5/CASB/175	1.187 ± 0.001	0.0166
	UF-CE0.5/175	1.207 ± 0.002	–
3	F-CE0.5/AZD/175	0.697 ± 0.053	0.4225
	UF-CE0.5/175	1.207 ± 0.002	–
4	F-CE2/CASB/175	1.162 ± 0.011	0.0333
	UF-CE2/175	1.202 ± 0.009	–
5	F-CE0.5/AZD/160	0.82 ± 0.008	0.3115
	UF-CE0.5/160	1.191 ± 0.009	–
6	F-CE2/AZDCASB/190	0.831 ± 0.056	0.3081
	UF-CE2/190	1.201 ± 0.001	–
7	F-CE2/AZD/190	0.534 ± 0.082	0.5554
	UF-CE2/190	1.201 ± 0.001	–
8	F-CE1/CASB/190	1.165 ± 0.004	0.0308
	UF-CE1/190	1.202 ± 0.003	–
9	F-CE1/CASB/190	1.144 ± 0.017	0.0482
	UF-CE1/190	1.202 ± 0.003	–
10	F-CE0.5/AZD/190	0.543 ± 0.072	0.5486
	UF-CE0.5/190	1.203 ± 0.001	–
11	F-CE2/AZD/175	0.807 ± 0.016	0.3552
	UF-CE2/175	1.202 ± 0.009	–
12	F-CE1/AZD/175	0.586 ± 0.058	0.5038
	UF-CE1/175	1.181 ± 0.015	–
13	F-CE2/AZDCASB/160	1.111 ± 0.026	0.0718
	UF-CE2/160	1.197 ± 0.001	–
14	F-CE0.5/AZDCASB/160	1.008 ± 0.042	0.1536
	UF-CE0.5/160	1.191 ± 0.009	–
15	F-CE2/CASB/175	1.16 ± 0.005	0.0349
	UF-CE2/175	1.202 ± 0.009	–
16	F-CE1/CASB/160	1.161 ± 0.006	0.0333
	UF-CE1/160	1.201 ± 0.003	–
17	F-CE1/AZD/190	0.553 ± 0.103	0.5399
	UF-CE1/190	1.202 ± 0.003	–
18	F-CE0.5/AZDCASB/190	0.926 ± 0.059	0.2303
	UF-CE0.5/190	1.203 ± 0.001	–
19	F-CE2/AZD/160	0.833 ± 0.016	0.3467
	UF-CE2/160	1.197 ± 0.001	–
20	F-CE1/CASB/160	1.163 ± 0.003	0.0316
	UF-CE1/160	1.201 ± 0.003	–

According to Table 5 and Fig. 2, the strongest impact on the foam void fraction belongs to the CFA type. The temperature profile of extruder takes the second place. Similar results have been reported in the previous works [14, 21, 22]. The RSM analysis reveals that the lightest PLA foam is extruded by incorporating the AZD foaming agent and adjusting the 190 °C temperature profile.

Table 4 ANOVA data of the fitted model for the void fraction response

Source	Sum of squares	Degree of freedom	Mean square	*F*-value	*P*-value	Significance
Model	0.79	5	0.16	115.75	< 0.0001	Significant
B-Temperature profile	0.058	1	0.058	42.74	< 0.0001	
C-CFA type	0.67	2	0.34	246.56	< 0.0001	
BC	0.026	2	0.013	9.48	0.0025	
Lack of Fit	0.019	10	1.887E − 003	47.30	0.0010	Significant

Table 5 Final fitted equations in terms of actual factors for void fraction response

CFA type	Fitted function
C1-AZD	$\text{Void fraction} = -0.85276 + 7.354 \times 10^{-3} \times \text{temperature profile}$
C2-AZD + CA/SB	$\text{Void fraction} = -0.72197 + 5.217 \times 10^{-3} \times \text{temperature profile}$
C3-CA/SB	$\text{Void fraction} = -0.01005 + 2.350 \times 10^{-4} \times \text{temperature profile}$

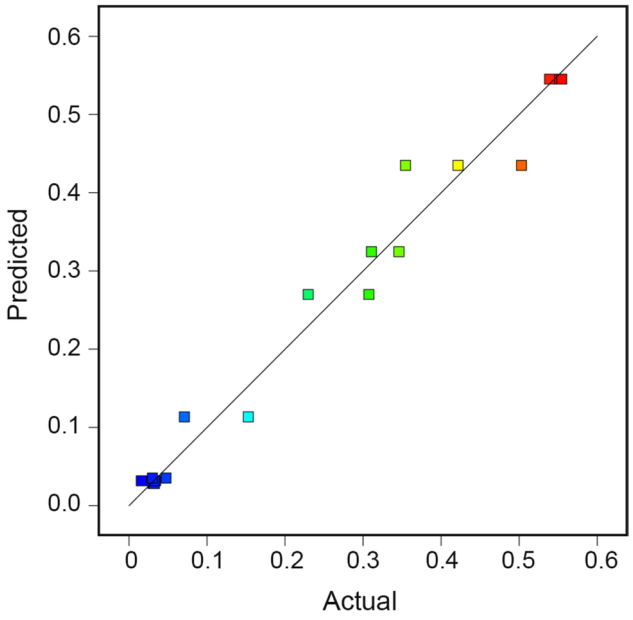

Fig. 1 Predicted values of void fraction versus actual values using linear interpolating function yielded from RSM

Physical and structural properties

As mentioned earlier, the densities and void fraction of the prepared samples are collected in Table 3. From the data in Table 3, it is clear that the density values decrease with the foaming process. According to the data in Table 3, among the foamed samples, the F-CE2/AZD/190 sample which was foamed at the highest processing temperature and contained the highest amount of chain extender as well as the exothermic foaming agent show the lowest density and the highest void fraction of 0.55.

For all the samples containing the endothermic foaming agents, the foam density is comparatively high and the void fraction is not considerable. For instance, the highest density and the lowest void fraction are observed for the sample containing CA/SB foaming agents prepared at the die temperature of 175 °C with 0.5 phr of chain extender, i.e., F-CE0.5/CASB/175 sample. The plausible reason is the lack of enough melt strength for the samples containing just CA/SB foaming agents to keep the gas created by the decomposition reaction of these foaming agents in the melt. Consequently, the gas escapes from the melt by rupturing the cell walls after exiting the die. Similar results were reported for the foams containing SB and CA [22]. However, for the samples in which AZD is applied along with CA/SB foaming agents, better performance of chemical foaming agents is observed.

An increment in CE content results in lower foam density and larger void fraction. It can be found by comparing the data for these pairs: F-CE0.5/AZD/175 sample with the same sample containing 1 phr of CE, F-CE0.5/AZD-CASB/190 sample with the same sample containing 2 phr of CE, and F-CE1/AZD/190 sample with the same sample containing 2 phr of CE. These results indicate that higher levels of CE, in the presence of AZD foaming agent, lead to improvements in the melt strength and preservation of gas molecules in the melt. Moreover, it is also observed that the void fraction of foams increases by applying larger die temperatures. This change is more noticeable in the foams in which the exothermic foaming agent, AZD, is used. This originates from more intensified decomposition of the foaming agents, especially AZD, at higher processing temperatures and the production of higher volumes of gas for the nucleation and growth of bubbles. The beneficial effects of applying higher melt temperature and larger CE content on the foamability of PLA were also reported by other groups [13, 15, 21]. In these works, the lightweight PLA foams with larger cell densities were attained at higher melt temperatures and larger CE contents.

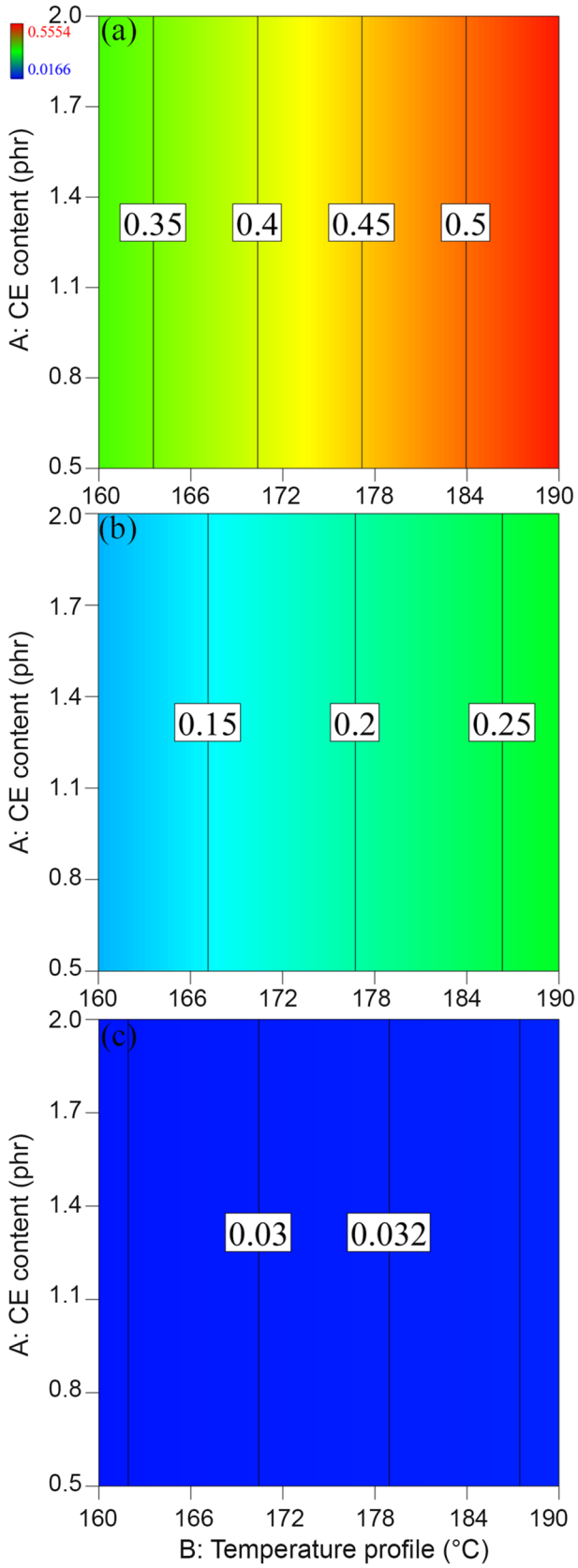

Fig. 2 Contour plots of void fraction against extruder temperature profile and CE content for different types of CFA: **a** AZD, **b** AZD + CA/SB, and **c** CA/SB

To investigate the effects of the variables studied here on the structural properties of foams, the SEM images of the cryo-fractured surfaces of samples were obtained. These images are shown in Fig. 3. The SEM images of Fig. S1 (in Supplementary materials) are shown with higher magnification for more details. As mentioned in the experimental part, some of the foams just contain CA/SB endothermic foaming agents. The cryo-fractured surfaces of these samples are shown by the micrographs (a), (b), (h), (i), (k), (m), (n), and (s) in both Fig. 3 and Fig. S1 (in Supplementary materials). In these microscopic images, it is evident that no holes are present on the surfaces of these samples. This is in accordance with the void fraction results of these foams, which are comparatively very small, compared to those of foams containing exothermic foaming agents.

As it is mentioned earlier, during the extrusion foaming process of the samples after leaving the die, the gas molecules resulting from the decomposition of foaming agents can escape from the melt by bursting the bubbles, which originate from the low melt viscosity and strength. The plausible reason for this is the presence of water molecules that are produced by CA/SB decomposition reaction [22]. As shown in the reaction scheme of Fig. 5, H_2O molecules facilitate the chain scission of the PLA matrix, hence deteriorating the melt strength of PLA and causing the bubble wall rupture and gas removal. However, bubbles at low densities can be discerned on the cryo-fractured surfaces of foams containing all three foaming agents, i.e. AZD/CA/SB. In Fig. 3 and Fig. S1 (in Supplementary materials), the SEM images related to these foams are: (f), (g), (o), and (r).

From the SEM images of Fig. 3 and Fig. S1 (in Supplementary materials), it is clear that the foams, in which AZD was used as a foaming agent alone, have the highest cell densities, which is in agreement with the findings of the previous works [22, 25]. The foam morphology here is crucially dependent on the type of foaming agents, exothermic or endothermic ones, regardless of the temperature profile of the extruder and content of the chain extender. By comparing the foams with the same formulation and different die temperatures, foam pairs with the SEM images of (f)/(g) and (r)/(o) in Fig. 3 and Fig. S1 (in Supplementary materials), it can be found that the cell density of samples obtained at higher temperature (190 °C) is larger. At higher processing temperatures, the AZD foaming agent is decomposed more intensely and the volume of the produced gas is larger, as expected. The higher volume of gas has created larger bubbles at higher quantities in the polymer matrix, which also results in lower densities as well [21, 22].

By using image analysis software on the SEM images of Fig. 3, the average size of foam bubbles including the number-average diameter (D_n) and volume-average diameter (D_V) along with the size distribution of bubbles (D_v/D_n) and

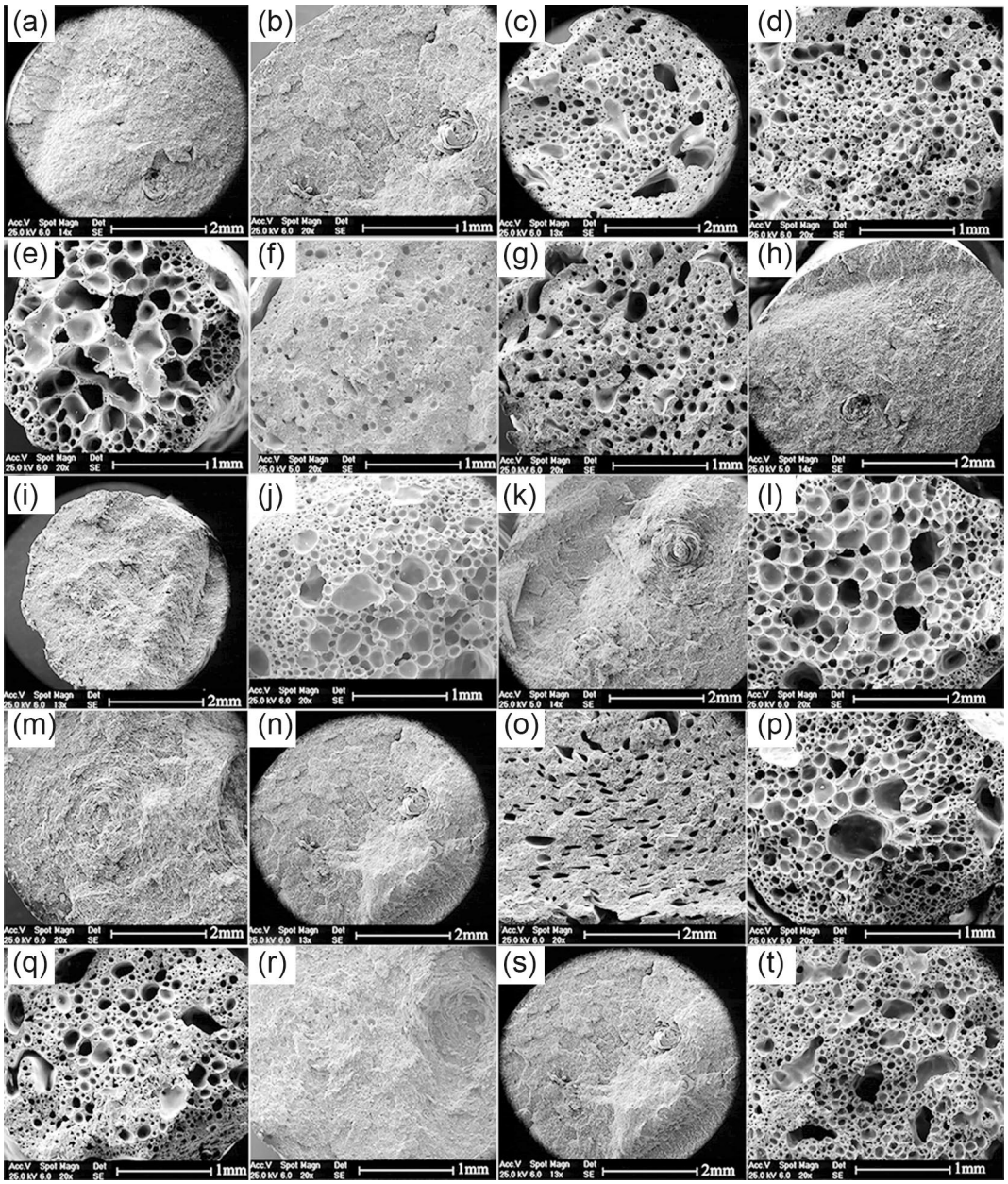

Fig. 3 SEM images of foam samples: **a** F-CE0.5/CASB/175, **b** F-CE0.5/CASB/175, **c** F-CE0.5/AZD/175, **d** F-CE0.5/AZD/160, **e** F-CE0.5/AZD/190, **f** F-CE0.5/AZDCASB/160, **g** F-CE0.5/AZD-CASB/190, **h** F-CE1/CASB/190, **i** F-CE1/CASB/190, **j** F-CE1/AZD/175, **k** F-CE1/CASB/160, **l** F-CE1/AZD/190, **m** F-CE1/CASB/160, **n** F-CE2/CASB/175, **o** F-CE2/AZDCASB/190, **p** F-CE2/AZD/190, **q** F-CE2/AZD/175, **r** F-CE2/AZDCASB/160, **s** F-CE2/CASB/175, and **t** F-CE2/AZD/160

cell density were calculated and the resultant data are gathered in Table 6. As can be seen, these data cannot be measured for some of the samples, which contain CA/SB foaming agents, because no bubble can be discerned on the corresponding SEM images of cryo-fractured surfaces. The data collected in Table 6 show that the foams having AZD foaming agent alone have higher cell densities than the foams containing a combination of CFAs, i.e. AZD, CA and SB.

By changing the foaming agents from AZD/CA/SB to AZD at a fixed CE level and die temperature, PLA foams with larger cell densities, smaller bubbles and less uniformity in bubble size were obtained. D_v/D_n of bubbles for the foams with AZD is larger than the foams containing AZD/CA/SB foaming agents obtained at fixed CE and temperatures. These results originate from the elimination of CA/SB

Table 6 The number-average diameter (D_n), volume-average diameter (D_v), bubble size distribution (D_v/D_n) and cell density of the PLA foams

No	Sample code	D_n (μm)	D_v (μm)	D_v/D_n	Cell density (cells/cm^3)
1	F–CE0.5/CASB/175	–	–	–	–
2	F–CE0.5/CASB/175	–	–	–	–
3	F–CE0.5/AZD/175	82.41	572.36	6.9	8.99×10^5
4	F–CE2/CASB/175	–	–	–	–
5	F–CE0.5/AZD/160	85.09	275.71	3.2	6.54×10^5
6	F–CE2/AZDCASB/190	95	238.36	2.5	2.75×10^5
7	F–CE2/AZD/190	84.41	545.68	6.5	9.15×10^5
8	F–CE1/CASB/190	–	–	–	–
9	F–CE1/CASB/190	–	–	–	–
10	F–CE0.5/AZD/190	82.1	294.7	3.5	3.98×10^5
11	F–CE2/AZD/175	70.38	371.44	5.3	7.18×10^5
12	F–CE1/AZD/175	112.08	464.87	4.1	9.96×10^5
13	F–CE2/AZDCASB/160	–	–	–	–
14	F–CE0.5/AZDCASB/160	100.4	286.6	2.9	4×10^4
15	F–CE2/CASB/175	–	–	–	–
16	F–CE1/CASB/160	–	–	–	–
17	F–CE1/AZD/190	108.94	332.98	3.0	7.30×10^5
18	F–CE0.5/AZDCASB/190	110.03	297.78	2.7	2.20×10^5
19	F–CE2/AZD/160	95.7	470.97	4.9	9.50×10^5
20	F–CE1/CASB/160	–	–	–	–

from the foam formulation and correspondingly, the absence of water byproduct and its deterioration effect on PLA foamability [14, 22].

By comparing the results presented in Table 6, it can be also found that the application of 190 °C for the die zone does not result in the largest bubbles and cell densities for the PLA foams with CE contents of 0.5 and 1 phr. At these levels of CE, the largest values of D_n, D_V, D_v/D_n and cell density are measured for the foams extruded at a die temperature of 175 °C. While, at a CE level of 2 phr, an increment in the die temperature from 175 to 190 °C brought about the extrusion of a PLA foam having higher cell density and larger bubbles with broader cell size distribution. Dinakaran et al. [21] reported that the higher extrusion temperatures caused the formation of more nucleation sites and further growth of bubbles. For CE levels of 0.5 and 1 phr, the largest D_v/D_n was obtained at 175 °C temperature, while the broadest cell size distribution was measured for 190 °C processing temperature at the CE content of 2 phr.

In the chemical extrusion foaming process of biodegradable PLA, several chemical reactions take place concurrently through continuous fluid flow. Although the higher process temperature results in more intensified decomposition of CFA, the weaker viscoelastic properties of PLA melt at this temperature cause less resistance of melt against the extensional flow field during the bubble growth stage. It is noteworthy that an improvement in the PLA melt strength at this temperature can be attained by incorporating more CE additive. The more intense activity of CE additive in PLA chain structure and molecular weight can compensate for more intensified chain scission of PLA at higher processing temperatures.

Another notable point of Table 6 is the effect of CE level on the cell size distribution for the samples foamed by incorporating AZD CFA at a fixed temperature profile. Comparing the related results of D_v/D_n for the foams, extruded at a certain temperature profile, clarifies that the cell size distribution becomes broader at higher CE content, namely 2 phr. The observed change originates from the stronger reaction of CE to change the molecular weight and chain structure of PLA at higher CE content. Because of this, less uniformity is obtained in the PLA melt viscoelastic properties, hence causing less uniformity in the bubble size.

Chemical reactions through extrusion foaming of PLA melt

Considering PLA as a biodegradable polymer that usually undergoes changes in molecular weight and structure during melt processing, investigating the chemical reactions during the extrusion foaming process of PLA in the presence of chain extender and chemical foaming agent is of great importance to control the process and correspondingly, the performance and properties of the foam [26]. The rheological properties of PLA melt are among the most important properties of PLA during the foaming process, which controls the growth of bubbles and foam morphology. The rheological properties of a polymer melt are profoundly impacted by its average molecular weight, molecular weight distribution, and chain structure [27]. These molecular characteristics are altered by the PLA chain scission reaction, chain extension reaction induced by CE additive, decomposition reaction of CFA/CFAs and melt temperature.

The number-average molecular weight (M_n), weight-average molecular weight (M_w) and dispersion index (PDI) for some of the prepared samples were obtained by GPC analysis and their corresponding results are listed in Table 7. As can be found from the data compared for UF-CE2/190 and F-CE2/AZD/190 samples, the PLA molecular weight diminishes and the molecular weight distribution becomes broader in the presence of AZD, an exothermic foaming agent. It clarifies that the chain scission reaction of PLA macromolecules is intensified by the occurrence of AZD

Table 7 Different average molecular weight values along with polydispersity index obtained from GPC analysis

Sample	$\overline{M}_n$(g/mol)	$\overline{M}_w$(g/mol)	$\overline{M}_z$(g/mol)	PDI
UF-CE2/190	6.93×10^4	1.26×10^5	2.11×10^5	1.82
F-CE2/AZD/190	5.90×10^4	1.15×10^5	2.07×10^5	1.95
F-CE2/CASB/175	7.69×10^4	1.38×10^5	2.31×10^5	1.80

decomposition reaction. The heat generated from the decomposition of AZD CFA during the foaming process heightens the melt temperature and consequently, decreases the molecular weight of PLA.

The effect of melt temperature on the chain scission reaction and molecular weight of PLA macromolecules can be also evaluated by comparing the GPC results of F-CE2/CASB/175 and F-CE2/AZD/190 samples in Table 7. The higher extruder temperature profile results in lower molecular weight of PLA chains. However, as mentioned before, the PLA foam samples that are prepared in the presence of CA/SB foaming agents have the lowest void fractions. During the extrusion foaming process of PLA, CA/SB foaming agents are decomposed at lower temperatures than AZD and water molecules are formed as side-products of the CA/SB decomposition reaction. Figure 4 shows the scheme of the CA/SB decomposition reaction. The presence of H_2O molecules in PLA melt can intensify the hydrolysis reaction of the polymer chains, which is shown in Fig. 5 [14, 22]. As a direct result of more intense chain scission, the molecular weight and melt strength of PLA have considerably reduced, hence deteriorating the foamability of the melt. In a research work conducted by Kmetty et al. [22], it has shown that no obvious foaming structure can be discerned for the extruded PLA foamed by applying endothermic foaming agents, owing to the deteriorating effect of the foaming agent.

When the samples containing CA/SB foaming agents were removed from the die of the extruder, severe gas removal from the melt, cell wall rupture and low viscosity and melt strength were observed. Furthermore, another piece of evidence that confirms the mechanism shown in Fig. 4 is the observation of water vapors and droplets on the inner wall surface of the extruder hopper, that is, when the PLA foaming process occurred by adding the citric acid and sodium bicarbonate foaming agents.

In contrast to the endothermic foaming agents, the decomposition reaction of AZD is not involved in the formation of water. The reaction scheme of AZD decomposition

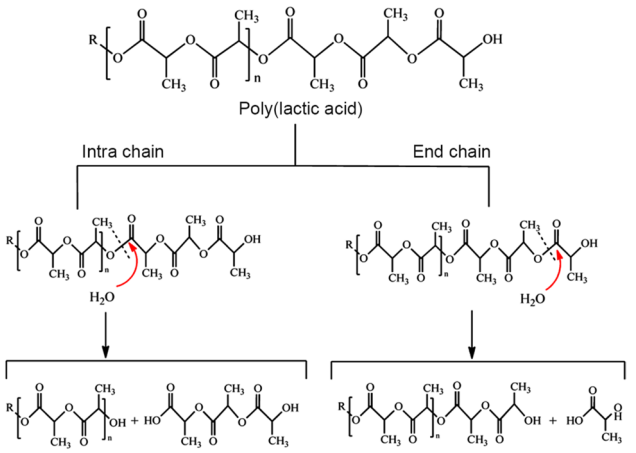

Fig. 5 The scheme of PLA hydrolysis and chain scission reaction in the presence of water

is represented in Fig. 6 [28]. Unlike CA/SB foaming agents, no water vapors and droplets were observed on the inner wall surface of the extruder hopper during the extrusion of PLA foams containing AZD foaming agent. In addition, N_2 molecules are very stable and AZD decomposes through a mechanism which results in stable N_2 molecules. In addition to this difference, the decomposition reaction of the exothermic and endothermic foaming agents used here begins at temperatures that are noticeably different.

To evaluate the decomposition temperatures and thermal stability of the raw materials used here in the processing conditions, TGA was employed. Figure 7 shows the thermal degradation of virgin PLA and other raw materials used. The thermal characteristics of the materials including onset and end-point temperatures of the degradation step along with the half-height temperatures, in which 50% of sample weight was lost, are collected in Table 8. As can be seen, thermal degradation of PLA chains occurs in the temperature range of 280–344 °C. The decomposition of this substance is mainly associated with the hydrolysis of ester groups in chain backbones and it is accelerated by the COOH groups present at the chain ends [29]. The thermal degradation of the chain extender occurs in one step. It starts from the temperature of 290 °C and continues up to the temperature of 431 °C. Both these polymers begin their thermal degradation at temperatures much higher than the processing temperatures, albeit in the absence of the fluid flow field.

The decomposition of AZD foaming agent happens in several steps. The first stage of decomposition begins at

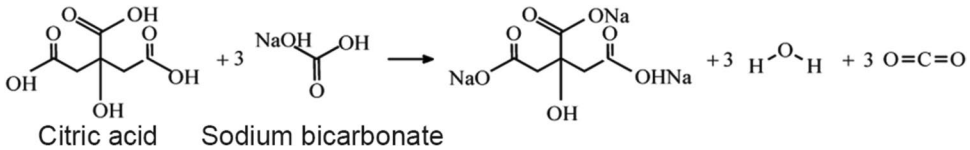

Fig. 4 The scheme of a decomposition reaction of citric acid and sodium bicarbonate

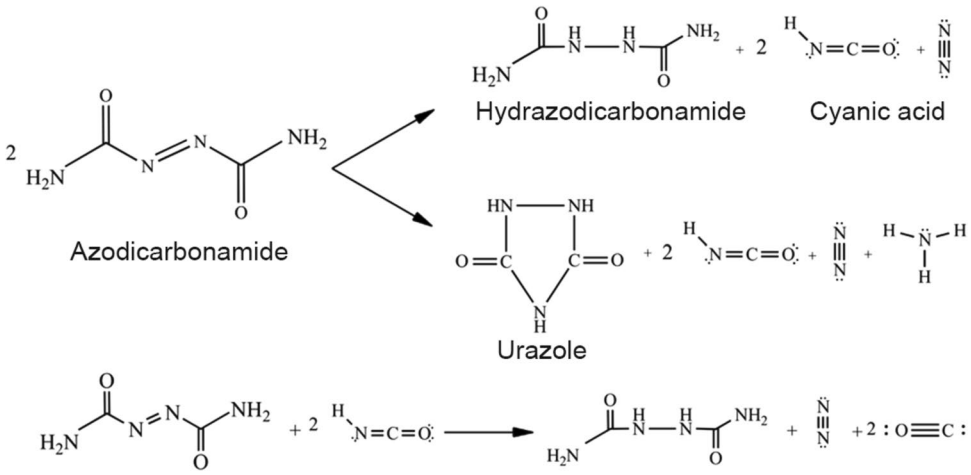

Fig. 6 The scheme of a decomposition reaction of azodicarbonamide

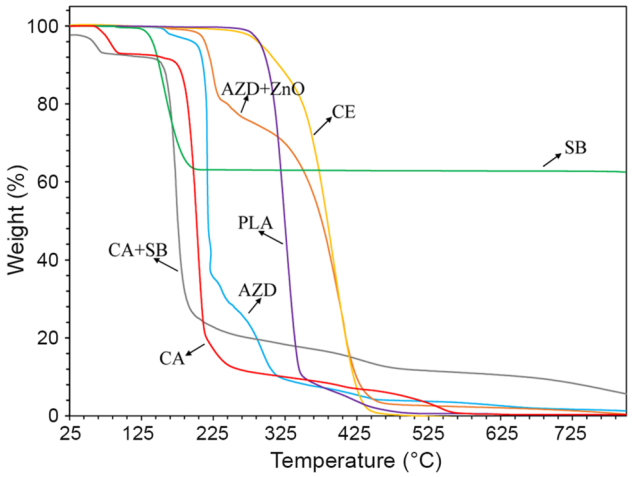

Fig. 7 TGA thermograms of raw materials used

Table 8 Data related to the thermal degradation of the used raw materials

Material	Onset temperature °C	Endpoint temperature °C	Temperature at half-height °C	Ash content (% by weight)
PLA	280	344	324	0.3
CE	290	431	384	0
AZD	200	433	375	1.3
AZD + ZnO	146	422	217	0.5
SB	128	184	159	62.5
CA	58	515	201	0.32
CA + SB	44	410	175	5.6

200 °C and involves the formation of carbon monoxide, nitrogen and urea, which is also shown in Fig. 6. The second stage of AZD decomposition occurs in the temperature range of 330–433 °C, which is accompanied by the production of ammonia and isocyanic acid residue from urea [22, 30]. However, the addition of ZnO to AZD exothermic foaming agent diminishes the degradation temperatures of AZD. Similarly, the mixture of AZD + ZnO also shows a two-step decomposition behavior. The first stage of decomposition is accompanied by a small weight loss at around 146 °C, and the second stage occurs at the temperature range of 200–422 °C. The results demonstrate that by adding the ZnO activator to AZD CFA, the decomposition of the exothermic foaming agent is accelerated and its decomposition temperature is well placed in the temperature range of the extrusion process [31].

The thermal decomposition of SB is a single-step process that starts at the temperature of 128 °C. In contrast, the thermal decomposition of CA, another component of endothermic foaming agents, involves in two stages. The first stage of CA decomposition occurs at 58 °C, which originates from water evaporation. The main stage of CA decomposition position is at the temperature range of 161–211 °C. A combination of these two foaming agents, CA plus SB, shows a partial weight loss step at 44 °C owing to water evaporation. At the second stage of degradation in the temperature range of 139–186 °C, thermal decomposition is accompanied by the release of CO_2 gas and H_2O vapors, which is also shown in Fig. 4 [32].

Considering the low decomposition temperatures of CA/SB CFAs as well as the extruder barrel temperatures at the first and second zones, i.e., 140 and 145 °C, it can be found that the decomposition of the endothermic foaming agents starts at the primary stages of the extrusion process. Therefore, the formed gases escape from the hopper zone of the extruder, which is not limited by the feeding mode of the applied twin-screw extruder. In the starved-feeding conditions, the screw channels of the extruder do not fill with material completely, hence allowing the gases to escape [27]. During the extrusion foaming of the samples containing SB/CA foaming agents, the escape of thin

white smoke from the hopper verifies the happening of this phenomenon. Additionally, the remaining part of the formed gases dissolved in the melt includes water molecules, which can accelerate the hydrolysis of ester groups of PLA chain backbones. As a result, the chain scission of PLA macromolecules can be intensified by the presence of dissolved water vapors. Thus, after exiting the die, the viscoelastic properties of PLA melt become weaker in such a way that the melt cannot resist the bubble wall rupture and gas removal from the melt anymore [14, 22].

To improve the processability and final properties of PLA-based products, an additive called chain extender can be added to the extrusion feed during the shaping process. Due to the similarity of this biodegradable polyester to other industrial polyesters, such as poly(ethylene terephthalate) (PET), common epoxy-based chain extenders of PET or other synthetic polyesters are often used during the extrusion process of PLA to maintain the average molecular weight high enough [13, 33]. Chemical reactions leading to the formation of long-branched PLA molecules or higher molecular weight PLA chains can compensate for the worsening effects of PLA chain scission reaction on the rheological behavior of the fluid during the foaming process, especially bubble growth stage [15].

During the extrusion process after leaving the die, the aforementioned extended chain structures of PLA can bring about higher melt strength and elasticity. Even the long-branched PLA molecules can induce extension-thickening rheological behavior to the melt, which provokes stronger melt resistance against the bubble wall rupture during the bubble growth stage [27]. As a result of stronger viscoelastic properties and melt strength, the presence of the chain extender leads to the preparation of extruded PLA foams with smaller cells, higher cell density and larger void fraction [34].

According to the capabilities of FTIR spectroscopy, this method has been used in this research to analyze the activity of chain extender additive in the prepared PLA foams. The FTIR spectra for PLA foams along with virgin PLA, CE, CA, SB, AZD and ZnO are given in Fig. 8. The FTIR spectrum of virgin PLA has several characteristic bands at wavenumbers of 3443, 2937, 1763, and 1452 cm^{-1}. The first three wavenumbers belong to the stretching vibrations of O–H, C–H and C = O bonds, respectively and the last wavenumber is related to the bending vibration of C-H bonds [35, 36].

Several characteristic bands can be identified in the spectrum of the AZD foaming agent (Fig. 8b). One of these characteristic bands is at wavenumber of 742 cm^{-1}, which belongs to the isocyanic (HNCO) bonding vibrations. The band at 1625 cm^{-1} is related to N–H bending vibrations. Other bands at 1116 and 1733 cm^{-1} belong to the vibrational movements of C–N and (C = O)N bonds, respectively. The broadband appearing at the wavenumber of 3331 cm^{-1} in the

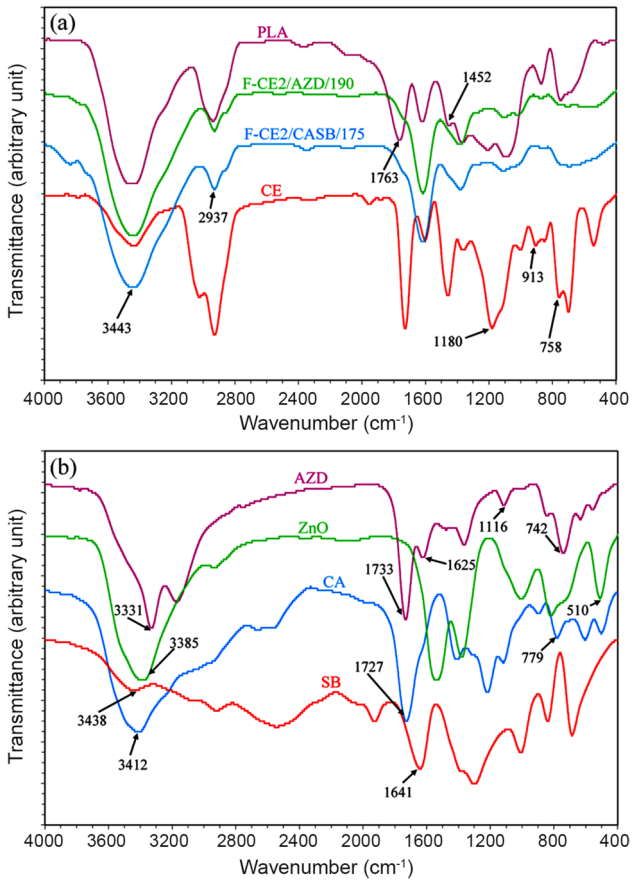

Fig. 8 **a** and **b** FTIR spectra for PLA foams along with virgin PLA, CE, CA, SB, AZD, and ZnO. The spectra are shifted along y-axis to better visualize the differences

AZD spectrum also originates from the stretching vibration of N–H bonds [37, 38]. The FTIR spectrum of ZnO powder has a characteristic absorption band at 510 cm^{-1}, which is related to the vibrations of the ZnO bond. Another band is also observed at 3385 cm^{-1}, which is related to the OH bond vibration, resulting from the absorption of atmospheric moisture [39]. In the spectrum of sodium bicarbonate, the band at 3438 cm^{-1} belongs to the stretching vibrations of OH bonds and the band at 1641 cm^{-1} is also related to the C = O vibrations [40].

In the spectrum of another component of endothermic foaming agent, namely, citric acid, the band at 3412 cm^{-1} corresponds to the stretching vibration of OH bonds, the band at 1727 cm^{-1} belongs to the vibration of C = O bonding and the band at 779 cm^{-1} corresponds to the vibration of CH_2 bonds [41]. In the FTIR spectrum of the chain extender in Fig. 8a, the absorption bands at wavenumbers 758, 913 and 1180 cm^{-1} are related to the vibrational movements of C–O–C bonds and ring of epoxy groups [42]. However, in the spectra of two foam samples, the above given absorption bands related to the bonding vibrations of epoxy groups

cannot be discerned. It can confirm the occurrence of the ring-opening reaction of the CE epoxy groups with the end groups of PLA chains. Due to the high reactivity of epoxy functional groups with hydroxyl and carboxyl end groups of PLA chains, especially at higher temperatures, new ether and ester groups form and the molecular weight of PLA chains increases [42]. However, the CE additive can also change the linear structure of PLA chains to long-branched and crosslinked structure. Among different chain-extended structures, the branched molecules having long chains linked to the primary PLA backbone are more effective in the improvement of rheological behavior of melt and foamability.

In order to determine the amount of crosslinked structure of PLA in the chain-extended foams, the gel contents of the foams extruded at the highest temperature profile were measured and gathered in Table 9. Gel formation demonstrates the creation of PLA crosslinks due to the addition of CE additive [43]. As can be found, the gel content of samples containing just CA and SB as foaming agents is higher than that of the samples containing exothermic foaming agent, AZD. Compared to the endothermic foaming agents, the presence of AZD foaming agent with an exothermic decomposition nature during the melt-mixing process leads to an increase in the melt temperature. Although higher melt temperatures result in more severe breakage of the polymer chains, lower melt viscosity causes better mixing of CE additive with melt and higher reactivity of epoxy functional groups. Therefore, more long linear chains and branched macromolecules are obtained by CE reaction in the foams containing AZD. Thereby, lower gel contents are observed in the samples containing AZD.

In the presence of the endothermic foaming agents, the CE activity has led to the formation of larger networks of PLA chains. For these foams, the melt temperature is lower. Higher melt viscosity as a result of lower melt temperatures and lesser amount of dissolved gases worsen the CE mixing conditions in the melt. Consequently, more crosslinked structures are formed by the CE reaction owing to the more non-uniform dispersion and distribution state of CE additive. In addition, it is clear in the table that the gel content of foams is heightened by increasing CE concentration. This phenomenon demonstrates that under appropriate conditions, CE can transform the structure of PLA chains from linear to longer linear, branched and network structures [15]. However, long linear chains and long-branched structures enhanced the melt strength of PLA considerably. For the PLA samples including the endothermic foaming agents, the advantageous effect of the chain extender additive is not strong enough to compensate for the impact of the PLA chain scission reaction.

Table 9 Gel content of different PLA foams extruded at 190 °C

Sample number based on formulation table (Table 2)	Sample code	Gel content (%)
6	F-CE2/AZDCASB/190	5.75 ± 0.01
7	F-CE2/AZD/190	4.13 ± 0.02
8	F-CE1/CASB/190	14.26 ± 0.01
9	F-CE1/CASB/190	10.0 ± 0.02
10	F-CE0.5/AZD/190	0.29 ± 0.02
17	F-CE1/AZD/190	2.07 ± 0.01
18	F-CE0.5/AZDCASB/190	2.14 ± 0.01

Conclusion

Currently, the effects of different material and processing variables, including the foaming agent type, chain extender concentration and extruder temperature profile on the physical and structural properties of PLA foams are evaluated. The results demonstrate that the lowest density, the highest void fraction and cell density, the smallest bubble size and more uniform cell size distribution are obtained in the PLA foams in the presence of AZD at highest CE level and extruder temperature profile. The largest void fraction, 0.55, was obtained for the F-CE2/AZD/190 sample. This sample showed a high cell density of 9.15×10^5 cells/cm^3. The statistical analysis of the foam properties by RSM verified that the largest void fraction of foams was obtained at the highest process temperatures in the presence of AZD. Additionally, the RSM analysis confirmed that the CFA type and extruder temperature profile are of great importance in controlling the foam properties.

Contrary to the foams containing AZD, the extruded PLA samples with the CA/SB foaming agents show high densities and low contents of bubbles. The TGA analysis confirmed the low decomposition temperature of CA/SB foaming agents, which leads to the escaping of gases from the hopper. Additionally, the presence of water as a by-product of the CA/SB decomposition reaction can bring about a more intense chain scission reaction of PLA chains.

Changes in the molecular weight of PLA chains in the extrusion foaming process were evaluated in the presence of chain extender and different foaming agents. GPC results showed that by foaming PLA, using the exothermic AZD foaming agent, the average molecular weight of PLA chains decreased. To evaluate the cross-linking degree of PLA at different loadings of CE, the gel content of the PLA foams was measured. The results of gel content analysis showed that the gel content of foams can increase by increasing the CE concentration. In the presence of endothermic foaming agents, the gel content of foams was relatively higher, confirming the presence of

more crosslinked PLA macromolecules. The advantageous effect of the chain extender reaction in changing the PLA molecular weight and structure is stronger for foams containing the AZD foaming agent. Higher extruder temperature is beneficial to intensify CE chain extension and AZD decomposition reactions.

The findings of this work clarify that PLA can be shaped into biodegradable foams by using a common industrial foaming process in a similar way as synthetic polymers like polystyrene. The prerequisites of extruding lightweight PLA foams are choosing the appropriate barrel and die temperatures, foaming agent type and chain extender level. By controlling the chemical reactions involved in the extrusion foaming process of PLA in the presence of CE and CFA, lightweight biodegradable foams with large cell densities can be achieved. This can expand the potential applications of the biodegradable thermoplastic PLA foams. However, adding nanoparticle and biodegradable elastomeric polymers to PLA will be beneficial for improving the foamability and final properties of the extruded PLA foams.

Supplementary Information The online version contains supplementary material available at https://doi.org/10.1007/s13726-024-01304-x.

Declarations

Conflict of interest The authors declare that there is no conflict of interest.

References

1. Singhvi M, Zinjarde S, Gokhal D (2019) Polylactic acid: synthesis and biomedical applications. Microbiol 127:1612–1626
2. Zhou L, Ke K, Yang MB, Yang W (2021) Recent progress on chemical modification of cellulose for high mechanical-performance Poly (lactic acid)/Cellulose composite: a review. Compos Commun 23:100548
3. Sarikhani K, Nasseri R, Lotocki V, Thompson R, Park C, Chen P (2016) Effect of well-dispersed surface-modified silica nanoparticles on crystallization behavior of poly (lactic acid) under compressed carbon dioxide. Polymer 98:100–109
4. Lee S, Kimoto M, Tanaka M, Tsuji H, Nishino T (2018) Crystal modulus of poly (lactic acid) s, and their stereocomplex. Polymer 138:124–131
5. Ramlee NA, Tominaga Y (2019) Mechanical and degradation properties in alkaline solution of poly (ethylene carbonate)/poly (lactic acid) blends. Polymer 166:44–49
6. Nofar M (2016) Effects of nano-/micro-sized additives and the corresponding induced crystallinity on the extrusion foaming behavior of PLA using supercritical CO_2. Mater Des 101:24–34
7. Sombatsompop N, Srimalanon P, Markpin T, Prapagdee B (2021) Polylactic acid (PLA): improve it, use it, and dump it faster. Bioresour 16:2196–2199
8. Kakroodi AR, Kazemi Y, Ding W, Ameli A, Park CB (2015) Poly (lactic acid)-based in situ microfibrillar composites with enhanced crystallization kinetics, mechanical properties, rheological behavior, and foaming ability. Biomacromol 16:3925–3935
9. Wang J, Chai J, Wang G, Zhao J, Zhang D, Li B, Zhao H, Zhao G (2019) Strong and thermally insulating polylactic acid/glass fiber composite foam fabricated by supercritical carbon dioxide foaming. Int J Biol Macromol 138:144–155
10. Castro-Aguirre E, Iniguez-Franco F, Samsudin H, Fang X, Auras R (2016) Poly (lactic acid): mass production, processing, industrial applications, and end of life. Adv Drug Deliv Rev 107:333–366
11. Litauszki K, Gere D, Czigany T, Kmetty Á (2023) Environmentally friendly packaging foams: investigation of the compostability of poly (lactic acid)-based syntactic foams. SM&T 35:e00527
12. Kuang T, Chen F, Chang L, Zhao Y, Fu D, Gong X, Peng X (2017) Facile preparation of open-cellular porous poly (*l*-lactic acid) scaffold by supercritical carbon dioxide foaming for potential tissue engineering applications. Chem Eng J 307:1017–1025
13. Nur Adilah AH, Ahmad S, Chen RS, Zailan F, Shahdan D (2019) Effect of processing temperature and foaming agent loading on properties of polylactic acid/kenaf fiber composite foam. Mater Today Proc 7:601–606
14. Litauszki K, Kmetty Á (2020) Characterization of chemically foamed poly (lactic acid). IOP Conf Ser Mater Sci Eng 903:012018
15. Tiwary P, Najafi N, Kontopoulou M (2021) Advances in peroxide-initiated graft modification of thermoplastic biopolyesters by reactive extrusion. Can J Chem Eng 99:1870–1884
16. Dörr D, Standau T, Murillo Castellón S, Bonten C, Altstädt V (2020) Rheology in the presence of carbon dioxide (CO_2) to study the melt behavior of chemically modified polylactide (PLA). Polymers 12:1108
17. Ludwiczak J, Kozlowski M (2015) Foaming of polylactide in the presence of chain extender. J Polym Environ 23:137–142
18. Julien J, Quantin JC, Bénézet JC, Bergeret A, Lacrampe M, Krawczak P (2015) Chemical foaming extrusion of poly (lactic acid) with chain-extenders: Physical and morphological characterizations. Eur Polym J 67:40–49
19. Su Y, Huang P, Sun J, Chen J, Zheng H, Luo H, Chong Y, Zhao Y, Wu F, Zheng W (2023) Extruded polylactide bead foams using anhydrous supercritical CO_2 extrusion foaming. J Appl Polym Sci 140:e54557
20. Wu H, Zhao G, Wang J, Wang G, Zhang W (2019) Effects of process parameters on core-back foam injection molding process. Express Polym Lett 13:390–405
21. Dinakaran I, Sakib-Uz-Zaman C, Rahman A, Khondoker MAH (2023) Controlling degree of foaming in extrusion 3D printing of porous polylactic acid. Rapid Prototyp J 29:1958–1968
22. Kmetty Á, Litauszki K, Réti D (2018) Characterization of different chemical blowing agents and their applicability to produce poly (lactic acid) foams by extrusion. Appl Sci 8:1960
23. Ataeefard M, Saeb MR (2015) A multiple process optimization strategy for manufacturing environmentally friendly printing toners. J Clean Prod 108:121–130
24. Ataeefard M, Sadati Tilebon SM, Reza Saeb M (2019) Intelligent modeling and optimization of emulsion aggregation method for producing green printing ink. Green Process Synth 8:703–718
25. Zimmermann MV, da Silva MP, Zattera AJ, Santana RM (2018) Poly (lactic acid) foams reinforced with cellulose micro and nanofibers and foamed by chemical blowing agents. J Cell Plast 54:577–596
26. Chen CQ, Ke DM, Zheng TT, He GJ, Cao XW, Liao X (2016) An ultraviolet-induced reactive extrusion to control chain scission and long-chain branching reactions of polylactide. Ind Eng Chem Res 55:597–605
27. Dealy JM, Wang J (2013) Melt rheology and its applications in the plastics industry. Springer Science & Business Media, Berlin

28. Reyes-Labarta J, Olaya M, Marcilla A (2006) DSC study of transitions involved in thermal treatment of foamable mixtures of PE and EVA copolymer with azodicarbonamide. Polym Sci 102:2015–2025
29. Chauhan S (2021) Effect of maleic anhydride grafted polylactic acid concentration on mechanical and thermal properties of thermoplasticized starch filled polylactic acid blends. Polym Polym Compos 29:S400–S410
30. Petchwattana N, Covavisaruch S (2011) Influences of particle sizes and contents of chemical blowing agents on foaming wood plastic composites prepared from poly (vinyl chloride) and rice hull. Mater Des 32:2844–2850
31. Lopez-Gonzalez E, Salmazo LO, Lopez-Gil A, Rodriguez-Perez MA (2019) Study of the effect of different electron irradiation doses on the decomposition temperature of azodicarbonamide. Polym Eng Sci 59:791–798
32. Bhiogade A, Kannan M, Devanathan S (2020) Degradation kinetics study of poly lactic acid (PLA) based biodegradable green composites. Mater Today Proc 24:806–814
33. Matuana L, Faruk O, Diaz C (2009) Cell morphology of extrusion foamed poly (lactic acid) using endothermic chemical foaming agent. Bioresour Technol 100:5947–5954
34. Zoski CG (2006) Handbook of electrochemistry. Elsevier, Amsterdam
35. Chen C, Ke D, Zheng T, He G, Cao X, Liao X (2021) Performance, interfacial compatibility testing and rheonaut technology analysis for simultaneous rheology and FTIR of poly (lactic acid)/modified saponite nanocomposites. Polym Test 100:107232
36. Herrera-Kao W, Loría-Bastarrachea M, Pérez-Padilla Y, Cauich-Rodríguez J, Vázquez-Torres H, Cervantes-Uc JM (2018) Thermal degradation of poly (caprolactone), poly (lactic acid), and poly (hydroxybutyrate) studied by TGA/FTIR and other analytical techniques. Polym Bull 75:4191–4205
37. Corre YM, Duchet J, Reignier J, Maazouz A (2011) Melt strengthening of poly (lactic acid) through reactive extrusion with epoxy-functionalized chains. Rheol Acta 50:613–629
38. Armentano I, Elena F, Nuria B, Franco D, Francesca L, Stefano F, Alfonso J, Kicheol Y, Jisoo A, Sangmi K, María KJ (2015) Processing and characterization of plasticized PLA/PHB blends for biodegradable multiphase systems. Express Polym Lett 9:583–596
39. Kooti M, Naghdi Sedeh A (2013) Microwave-assisted combustion synthesis of ZnO nanoparticles. J Chem 2013:562028
40. Shailesh J, Kalyanasundaram S, Balasubramanian V (2013) Quantitative analysis of sodium carbonate and sodium bicarbonate in solid mixtures using Fourier transform infrared spectroscopy (FTIR). Appl Spectrosc 67:841–845
41. Pichitchai P, Sumang R, Choopun S (2018) Effect of concentration of citric acid on size and optical properties of fluorescence graphene quantum dots prepared by tuning carbonization degree. Chiang Mai J Sci 45:2005
42. Sun Q, Mekonnen T, Misra M, Mohanty AK (2016) Novel biodegradable cast film from carbon dioxide based copolymer and poly (lactic acid). Polym Environ 24:23–36
43. Li Y, Mi J, Fu H, Zhou H, Wang X (2019) Nanocellular foaming behaviors of chain-extended poly (lactic acid) induced by isothermal crystallization. ACS Omega 4:12512–12523

Authors and Affiliations

Maryam Valipour[1] · Mahdi Rahmanifard[2] · Navid Jaberi[3] · Alireza Shadman[4] · Mehdi Hatami[1] · Hossein Ali Khonakdar[3] · Farkhondeh Hemmati[2]

✉ Mehdi Hatami
Hatami@ubonab.ac.ir

✉ Farkhondeh Hemmati
f.hemmati@ut.ac.ir

[1] Department of Polymer Science and Engineering, University of Bonab, Bonab, Iran

[2] Caspian Faculty of Engineering, College of Engineering, University of Tehran, Guilan, Iran

[3] Department of Polymer Processing, Iran Polymer and Petrochemical Institute, Tehran, Iran

[4] Department of Industrial Engineering, Ferdowsi University of Mashhad, Mashhad, Iran